IPP CERN Summer Student 2010 Project Report

Sébastien Picard
CERN - European Organization for Nuclear Research
385 route de Meyrin
Geneva, Switzerland

Project supervised through
Université de Montréal

31 August 2010

Preface

During my IPP CERN Summer Student fellowship I worked on two separate projects. For the first two months of the summer I was in Prof. Claude Leroy's group at Université de Montréal working on the estimation of neutron fluxes in the ATLAS cavern using Medipix detectors. I spent the second half of the summer at CERN, and while I kept working on neutron fluxes, I also began another project with Dr. Hulya Guler involving correlations in soft-QCD interactions in ATLAS minimum bias events. Accordingly, this report has been split into two sections.

Contents

Chapter 1

Estimate of Neutron Fluxes Using ATLAS-MPX Detectors

1.1 Introduction

Fifteen Medipix2-USB detectors have been placed in the ATLAS detector and cavern at the LHC at CERN. These detectors can measure, in real-time, radiation fields created by charged particles, photons and neutrons around ATLAS. Also, placing the Medipix detectors inside and outside ATLAS can give an indication of calorimeter leakage.

Neutrons are produced at ATLAS when particles coming from the collision point interact with the material of the detector. These neutrons can be of health and safety concern for people working outside the ATLAS cavern. Neutrons can also damage the pixel detectors in ATLAS; most of this damage is caused by displacement of the crystal atoms after exposure to neutron radiation. Measuring these neutron fields could also validate Monte Carlo simulations of particle interactions with the material inside the ATLAS detector.

For these reasons, it is of interest to obtain an estimate of the neutron fields in ATLAS. The efficiency of our neutron detectors must be calculated in order to do this. This project investigates the neutron detection efficiency of the Medipix detectors in ATLAS.

1.2 Description of Technique

1.2.1 The Medipix Detector

The Medipix2-USB detector is a 300-μm thick hybrid silicon detector. The active area of the detector spans 55x55 μm^2 and consists of 256x256 pixels. The sensor layer is bumpbonded to the electronics consisting of CMOS pixel readout chips. Incident radiation ionizes the silicon and creates electron-hole pairs; the holes drift to the cathode, and the energy is collected. An energy threshold is set for each individual pixel, and if the collected energy is over this threshold, then the pixel counts a signal. The device is read out by a Universal Serial Bus (USB) interface. Data is separated into frames, which contain the pixel information obtained during the acquisition time. The acquisition time must be short enough to prevent overlapping signals.

1.2.2 Converter Layers

Bare silicon cannot be used for neutron detection. However, the silicon active area of the Medipix detector can be coated with a converter layer to make the detector sensitive to neutrons. Incoming neutrons can interact with this converter layer and emit heavy charged particles, which are then detected by the silicon. The ATLAS-MPX detectors which are placed in the ATLAS detector are Medipix2-USB detectors covered with the layer shown in figure 1.1.

^{6}LiF is used for detecting slow neutrons (energy less than 1 MeV). It interacts with neutrons via neutron capture: $^6\text{LiF} + \text{n} \rightarrow \alpha + {}^3\text{H}$ with a cross section of 950 barns for 25meV neutrons. As the energy of the neutrons increases, the cross section for this interaction decreases significantly. For fast neutrons (energy

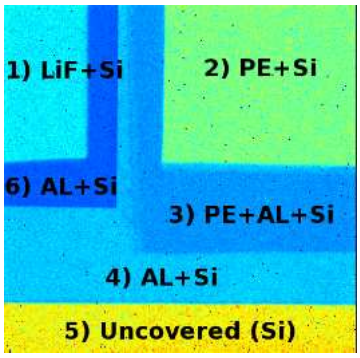

Figure 1.1: ATLAS-MPX Converter Layers: 1) LiF (5 mg/cm^2), 2) Polyethylene (PE) 1.3 mm thick, 3) PE (1.3 mm) layer above aluminium (100 μm), 4) Aluminium (100 μm), 5) Uncovered silicon and 6) Aluminium (150 μm).

greater than 1MeV), polyethylene is used for neutron conversion. This material is hydrogen-rich, which permits elastic collisions between the neutrons and the light hydrogen atoms: ^{1}H(n,n)p. The recoiling protons can then be detected in the underlying silicon layer. Aluminium layers are used to block background photons and electrons and to act as a kinematic threshold for the charged recoils.

1.2.3 High and Low Thresholds

The ATLAS-MPX detectors can operate in two energy threshold modes: high (230 keV) and low (8 keV). In high-threshold mode, it is assumed that only heavy charged particles leave a signal, such as charged recoils from neutron conversion reactions. The detector can therefore operate in counting mode, where all signal clusters are registered, regardless of their shape.

The low-threshold is the lowest possible threshold which excludes electronics noise. At low-threshold, signals are produced not only by neutrons, but also by light charged particles and photons. The detector response must be analysed with a pattern recognition algorithm to distinguish these signals.

The ROOT analysis package MAFalda developed by J. Idarraga at Université de Montréal was used for the data analysis. Pixel clusters are identified, and they are categorized depending on a set of parameters. In low-threshold mode, the signals corresponding to charged recoils coming from neutron interactions in the converter layers are categorized as "Heavy Blobs" for normal incident angle or "Heavy Tracks" for parallel incident angle. To analyse neutron fluxes with MAFalda in low-threshold mode, one must count these heavy tracks and heavy blobs.

1.2.4 Detector Efficiency

Data taken in 2009 at Czech Metrology Institute (CMI) [5] was used to determine the neutron detection efficiency. Two neutron sources were used: ^{241}AmBe with a mean neutron energy of 4.08 MeV and ^{252}Cf with 2.13 MeV. By varying the distances of these sources to the detector, various mean energies between 2 MeV and 4 MeV were obtained. More information on the experimental setup is provided in [4].

For each region, the efficiency was plotted against neutron energy, and the mean efficiency was determined. This efficiency was then used to calculate neutron fluxes for the ATLAS-MPX detectors in the unknown neutron field of ATLAS. To calculate the conversion efficiency of the polyethylene and LiF regions, a subtraction method was used. The number of registered neutron-like events in the uncovered silicon were normalized and subtracted from the normalized number of registered neutron-like events in the PE (or LiF) region. In low-threshold mode, registered neutron-like events were "Heavy Blobs" and "Heavy Tracks" as identified by MAFalda's pattern recognition algorithms. In high-threshold mode, all clusters were identified as registered neutron-like events.

For example, the efficiency of polyethylene at a given energy is expressed as:

$$\varepsilon(PE) = \frac{\frac{n_{PE+Si}}{A_{PE+Si}} - \frac{n_{Si}}{A_{Si}}}{\phi t}, \tag{1.1}$$

where n_{PE+Si} is the number of registered neutron-like events in the PE region, n_{Si} is the number of registered neutron-like events in the uncovered silicon, A is the area of the region, ϕ is the theoretical flux and t is the acquisition time.

1.3 Discussion

1.3.1 Efficiency Results

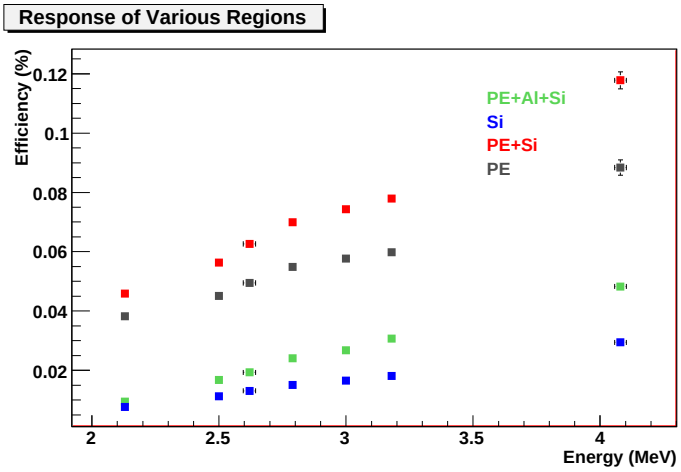

Figure 1.2: High-Threshold PE Efficiency Results

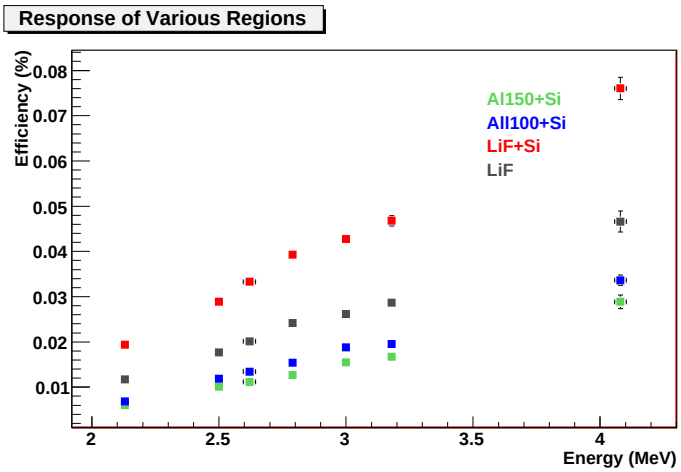

Figure 1.3: High-Threshold LiF Efficiency Results

The results for the neutron efficiency of various regions are shown in figures 1.2 to 1.5. Efficiencies labelled PE+Si and LiF+Si include all neutron-like events detected in the silicon beneath the PE and LiF regions. To obtain the efficiencies labelled PE and LiF, the normalized number of neutron-like events found in the uncovered silicon region were subtracted, as in equation 1.1. This represents the conversion efficiency of only the converter layer, without the background interactions occuring in silicon (which we assume are not neutrons).

High-Threshold Efficiency
In high-threshold mode, as the kinetic energy of the neutrons increases, the detection efficiency increases. This is caused by an increase in kinetic energy of the secondary particles produced in interactions which increases the probability of leaving a signal. For the polyethylene region, this is caused by the increase in

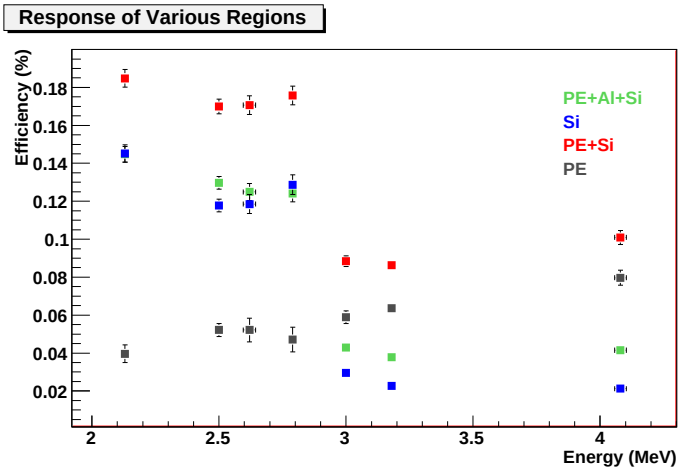

Figure 1.4: Low-Threshold PE Efficiency Results

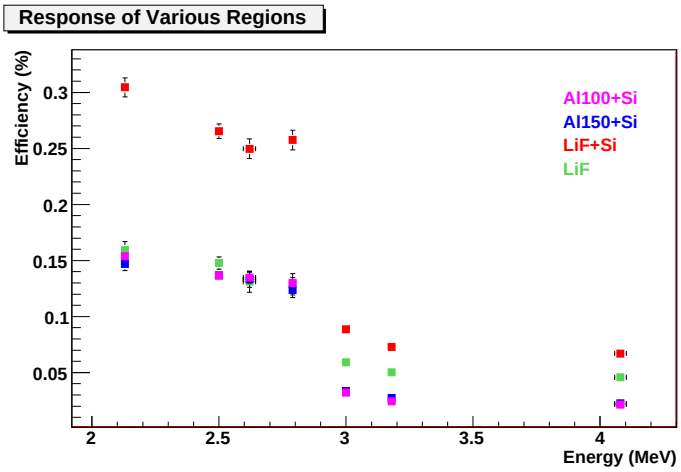

Figure 1.5: Low-Threshold LiF Efficiency Results

energy of recoil protons after the neutrons collide with polyethylene atoms. As the neutron's energy increases, more of these recoils have sufficient energy to trigger a signal in the Medipix pixel.

Low-Threshold Efficiency
One would expect efficiencies in low-threshold mode to be consistent with those found in high-threshold mode. However, only the polyethylene region efficiency is consistent in both threshold modes. For the LiF region, the efficiency decreases with increasing energy. This may be caused by overlapping of clusters in each frame. Reducing the acquisition time would help avoid this problem. Also, low energy alpha particles emitted from the neutron capture may not be distinguishable from the background of photons and electrons in MAFalda's pattern recognition algorithms.

1.3.2 Estimates of Neutron Fluxes in ATLAS

Recent data from the ATLAS-MPX detectors was analysed regularly using MAFalda. Frames from a given time period were downloaded and MAFalda was used to count the total number of neutron-like events in each region. These counts were normalized with respect to area, and for LiF and PE regions the normalized number of counts in silicon was subtracted. The mean efficiency calculated in the previous section was then applied to obtain a value for neutron fluence. Note that these estimates are done by supposing a homogeneous and isotropic neutron cloud in the ATLAS cavern. Some preliminary results for MPX detectors running in low-threshold mode are shown in figure 1.6.

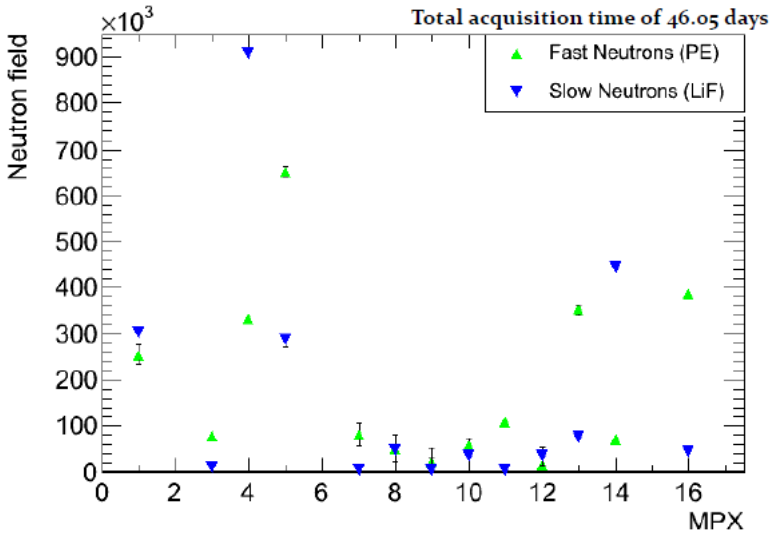

Figure 1.6: Preliminary Neutron Flux Results. Figure obtained from O. Scallon, 2010 [7]

The fluence obtained from the LiF region gives an indication of the number of thermal neutrons, while the fluence obtained from the polyethylene region indicates the number of fast neutrons. It is expected that ATLAS-MPX detectors surrounded by light material should detect more thermal neutrons than fast neutrons because of thermalization, an effect where neutrons bump into the light atoms and achieve thermal equilibrium through elastic collisions.

Results are still preliminary and are being analysed; however, a few observations can be made. ATLAS-MPX detectors which are close to the collision point such as MPX14 and MPX01 measure more neutrons during LHC collision time. Detectors such as MPX10 which check for radiation background in the cavern are far from the collision point and detect fewer neutrons than MPX14 during collision time.

1.4 Conclusions

Neutron detection efficiencies of ATLAS-MPX detectors have been determined using the pattern recognition algorithm of the MAFalda framework. These efficiencies were used to estimate the unknown neutron fields in ATLAS. Possible directions for the future include trying to correlate neutron fluxes with luminosity and varying acquisition time to reduce frame overlap.

Chapter 2

Effect of Systematic Errors in Factorial Moment Analyses in ATLAS Minimum Bias Events

2.1 Introduction

Event-to-event fluctuations in hadron collisions can provide an insight on the underlying soft quantum chromodynamics (QCD) processes. Large particle multiplicities in small rapidity regions for single events have been found to occur in experiments such as JACEE in 1983 [3]. However, these spikes could get washed out if only the rapidity distribution of the entire data set is examined.

It was proposed by Bialas and Peschanski in 1986 [2] that these fluctuations could be caused by intermittency in particle production. It is therefore important to identify fluctuations of physical origin and differentiate them from purely statistical fluctuations which may occur in single events. The solution proposed by Bialas and Peschanski was to study the normalized factorial moments of the multiplicity distribution as a function of the resolution. If the fluctuations are statistical, then the factorial moments will be constant as the resolution is changed. Any dependence of the moments on the resolution is a sign of genuine fluctuations of dynamical origin.

Moreover, measured factorial moments often disagree with Monte Carlo models [1]. Studying factorial moments may help improve our understanding of soft-QCD interactions.

The factorial moments may be sensitive to track loss and track duplication. It is therefore important to ensure that any observed dependence of the measured factorial moments on the resolution is not enhanced or diluted significantly by such effects. This project investigates the variation of the factorial moments when particle tracks are randomly deleted or duplicated.

2.2 Description of Technique

2.2.1 The Normalized Factorial Moment

For a given event, the pseudorapidity (η) space, $|\eta| < 2.5$, is divided into M bins. The definition of the normalized factorial moment of order q is as follows:

$$F_q = \frac{1}{M}\sum_{m=1}^{M}\frac{\frac{1}{N}\sum_{i=1}^{N} n_{mi}^{[q]}}{(\frac{1}{N}\sum_{i=1}^{N} n_{mi})^q}, \tag{2.1}$$

where $n_{mi}^{[q]} = n_{mi}(n_{mi}-1)...(n_{mi}-q+1)$ is the qth factorial moment of n_{mi}, i runs over the N events, and m runs over the M bins.

If the fluctuations are statistical, then F_q will be constant as the resolution M is varied. Power-law behaviour of the factorial moments as a function of M indicates intermittent effects of physical origin.

2.2.2 Data Sample

This analysis was done using ATLAS data collected at a centre-of-mass energy of $\sqrt{s} = 900$ GeV. The event and track selection criteria are as follows:

Event Selection
The only runs considered were those in which the inner detector was fully operational. Also, the L1_MBTS_1 trigger had to be satisfied. The event had to contain a vertex with ≥ 3 tracks. To be selected, an event had to contain at least one selected track.

Track Selection
The following criteria had to be satisfied for a track to be selected: $|\eta| < 2.5$, $p_t > 500$ MeV, $|d_0| < 1.5$ mm, $|z_0 \sin\theta| < 1.5$ mm. The track needed at least 1 pixel hit and at least 6 SCT hits. The track must have also been reconstructed by the "inside-out" tracking algorithm.

2.2.3 Systematic Errors

Systematic errors in data processing may create unphysical correlations or dilute existing physical correlations. The factorial moments depend on the multiplicity of tracks in a given η bin, and errors in track recognition will affect the factorial moments. It is important to know the extent to which the moments are sensitive to systematic track recognition errors. Three types of systematic errors were studied: track removal, track multiplication and track multiplication with smearing.

Track Removal
A fraction of the tracks was randomly removed from the analysis. This simulated missing tracks, which may remove a physical correlation.

Track Multiplication
A fraction of the tracks was randomly doubled. This simulated reconstructing a single track multiple times. A systematic duplication of tracks could produce a correlation which is not of physical origin.

Track Multiplication with Smearing
A fraction of the tracks was duplicated and then smeared according to a Gaussian distribution. This was done to investigate the effect of reconstructing a single track multiple times, given our resolution. The track pseudorapidity was changed randomly using a Gaussian distribution with variance of 0.01, which is the estimated resolution.

The Gaussian distribution was generated using the Box-Muller method. Two variables x_0 and y_0 are chosen randomly from a uniform distribution between -1 and 1. If $r_0^2 = x_0^2 + y_0^2 > 1$, then the values are discarded, and two new values are chosen. When two suitable values for x_0 and y_0 are found, then the following two values will follow a Gaussian distribution centred at 0 and of variance 1:

$$x = \sqrt{\frac{-2\ln r_0^2}{r_0^2}} x_0, \tag{2.2}$$

$$y = \sqrt{\frac{-2\ln r_0^2}{r_0^2}} y_0. \tag{2.3}$$

To change the mean to a given value μ and the variance to a given value σ, the following formula can be used: $\sigma x + \mu$.

2.3 Discussion

2.3.1 Track Removal

Figures 2.1 to 2.4 show the factorial moments as tracks are randomly removed. The moments generally decrease as tracks are removed, and there is little change when 1% of tracks are removed. The fractional decrease is relatively constant with M, and is much smaller than the percentage of tracks which were removed

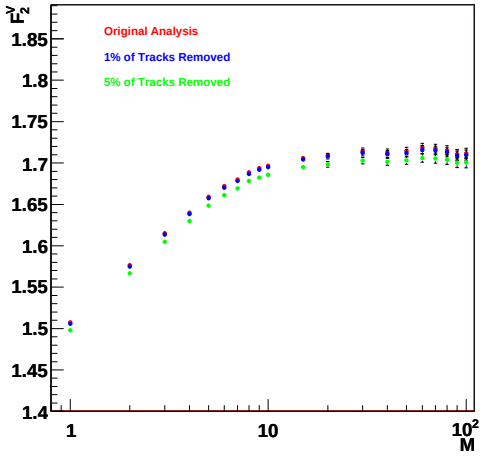

Figure 2.1: 2nd Order Moment: Track Removal

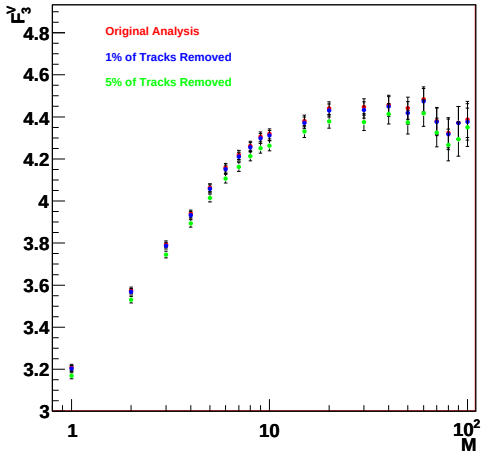

Figure 2.2: 3rd Order Moment: Track Removal

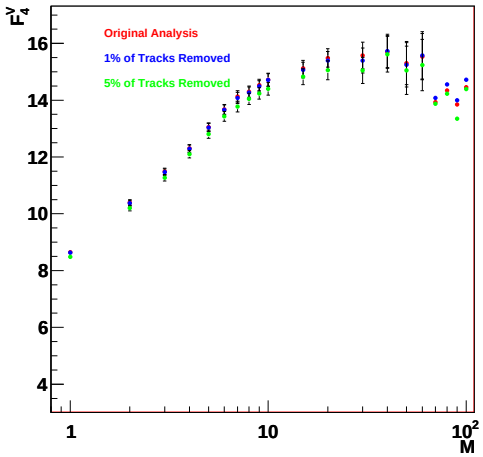

Figure 2.3: 4th Order Moment: Track Removal

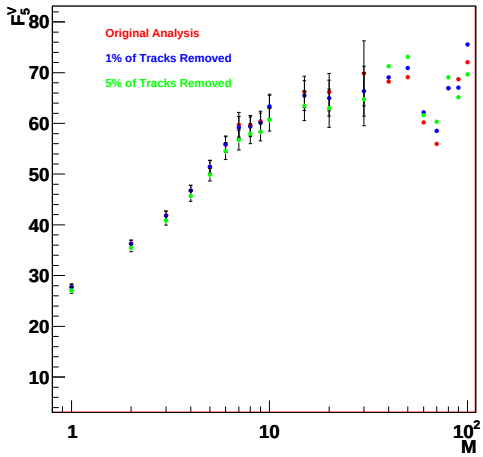

Figure 2.4: 5th Order Moment: Track Removal

(figures 2.5-2.8). The fractional difference in factorial moments is expressed as $(F_{\text{before}} - F_{\text{after}})/F_{\text{before}}$, where "before" and "after" signify before and after track removal.

For example, when 5% of the tracks are removed, the fractional change in the second-order moments is less than 0.5% (figure 2.5). The overall shape of the curve is generally preserved, which is important because intermittent processes are indicated by a dependence of the factorial moments on M.

For the higher-order moments, as M increases, the moments begin to act strangely. This is caused by the empty bin effect: as M increases, the average number of tracks per bin becomes small. If the average number of tracks per bin is smaller than the order of the moment, the measured factorial moments will fluctuate. This effect can therefore be expected to become more severe at large M and q. More information on the empty-bin effect can be found in the paper by P. Lipa et al. (1991) [6].

2.3.2 Track Multiplication

All orders of factorial moments diverge quite rapidly when 5% of the tracks are duplicated, as seen in figures 2.9-2.12. Even when as few as 1% of tracks are duplicated, the factorial moments significantly deviate from the original values at large M. This emphasizes how sensitive factorial moments are to track recognition. Systematic duplications will skew results and must be taken seriously.

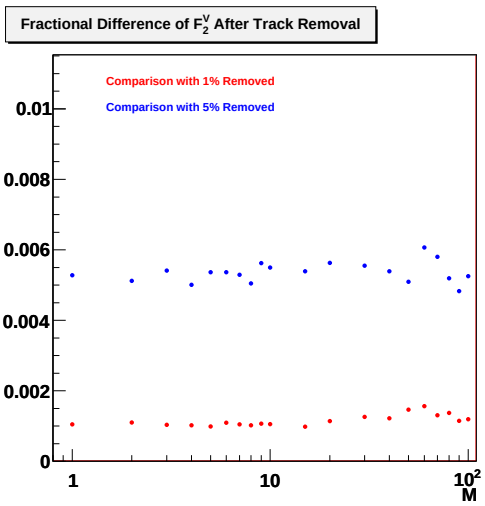

Figure 2.5: 2nd Order: $(F_{\text{before}} - F_{\text{after}})/F_{\text{before}}$

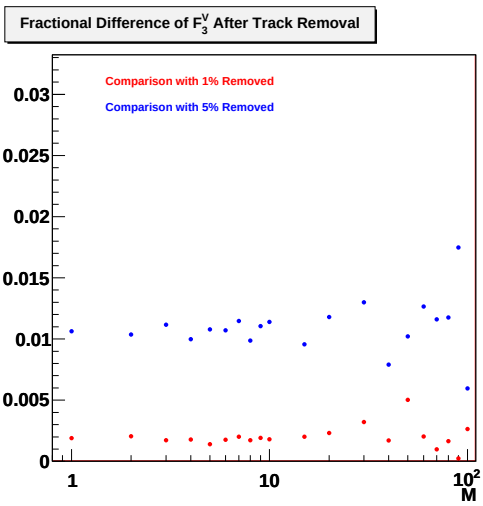

Figure 2.6: 3rd Order: $(F_{\text{before}} - F_{\text{after}})/F_{\text{before}}$

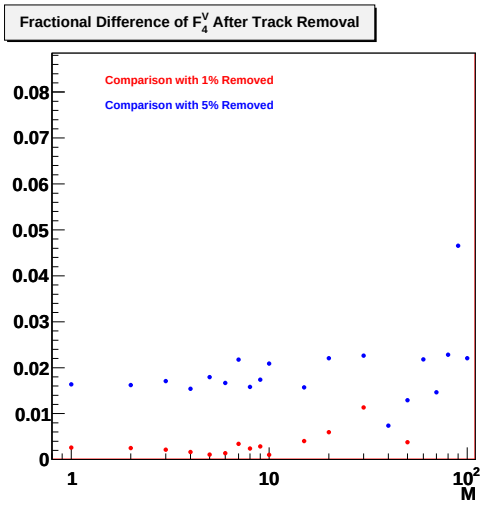

Figure 2.7: 4th Order: $(F_{\text{before}} - F_{\text{after}})/F_{\text{before}}$

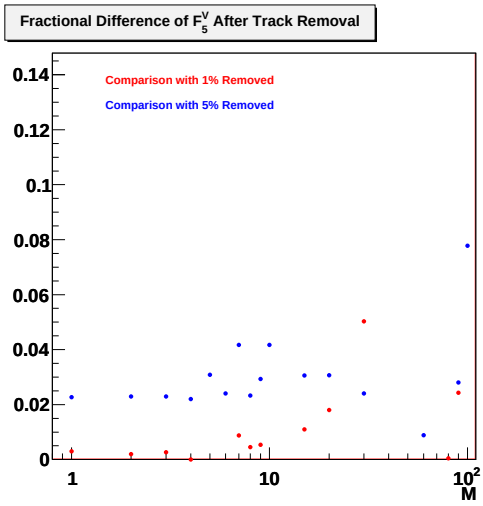

Figure 2.8: 5th Order: $(F_{\text{before}} - F_{\text{after}})/F_{\text{before}}$

2.3.3 Track Multiplication with Smearing

The factorial moments also rapidly diverge when tracks are duplicated and smeared. Tracks are duplicated within our resolution, and smearing within this resolution does not change the moments very much when compared to exact duplication. This can be understood by noting that the resolution in η (0.01) is much smaller than the width of the smallest bin (0.05).

2.4 Conclusions

The effect of certain systematic errors on normalized factorial moments was investigated. The random removal of 1% and 5% of tracks slightly decreased the factorial moments, and for a given order the fractional decrease was constant in resolution M.

Future goals include looking at track removal for only nearby tracks and track removal with an η and p_t dependence, instead of a purely random track removal.

The random duplication of 1% and 5% of tracks had a strong effect on the factorial moments for high resolutions. The next step should be to perform Monte Carlo studies to estimate the fraction of duplicated tracks, to ensure that this effect is not biasing our results.

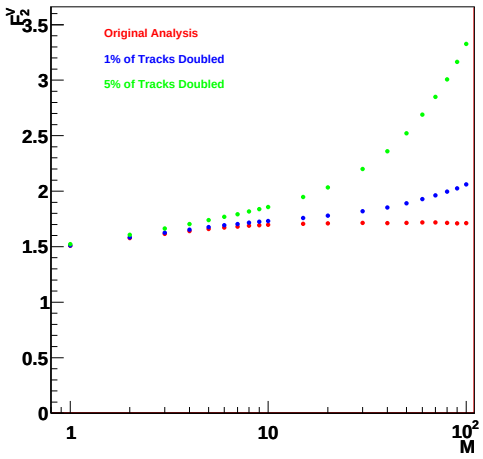

Figure 2.9: 2nd Order Moment: Track Duplication

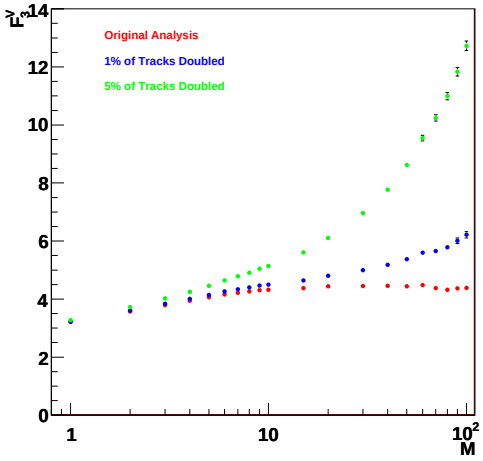

Figure 2.10: 3rd Order Moment: Track Duplication

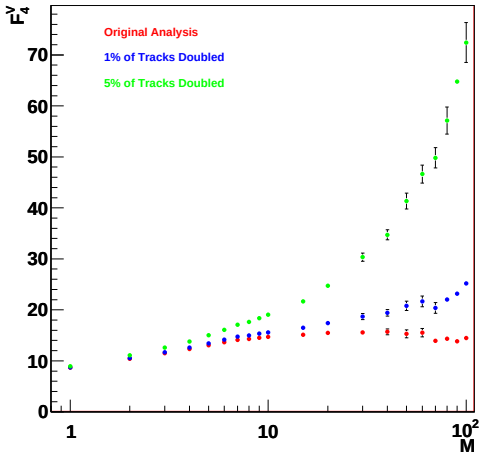

Figure 2.11: 4th Order Moment: Track Duplication

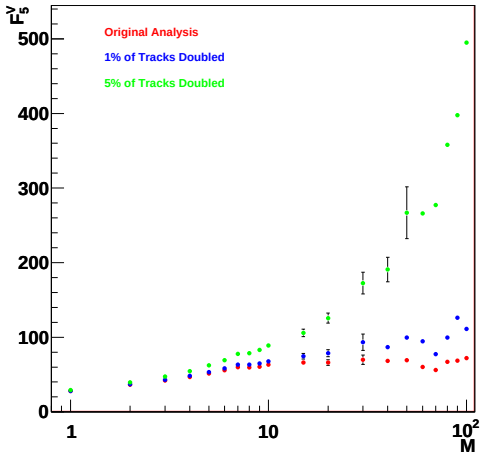

Figure 2.12: 5th Order Moment: Track Duplication

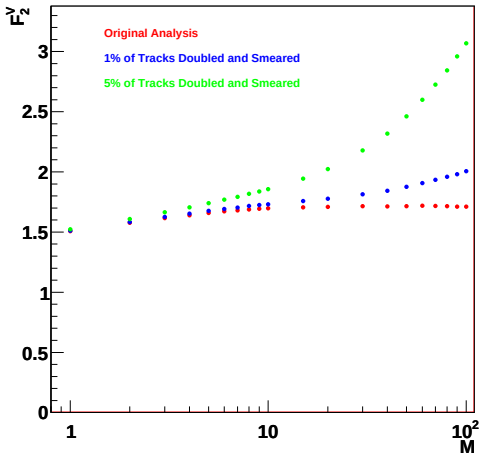

Figure 2.13: 2nd Order Moment: Track Duplication and Smearing

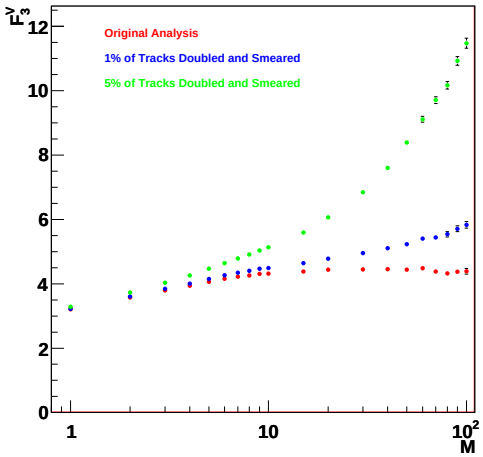

Figure 2.14: 3rd Order Moment: Track Duplication and Smearing

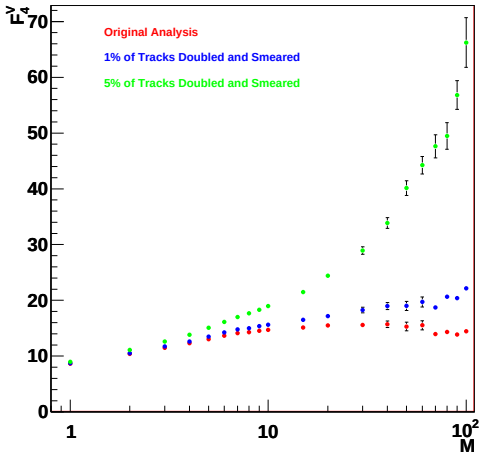

Figure 2.15: 4th Order Moment: Track Duplication and Smearing

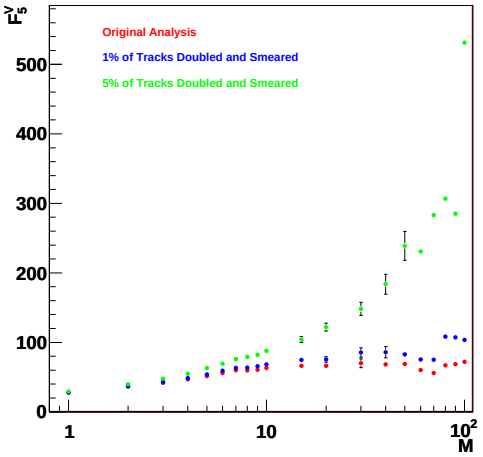

Figure 2.16: 5th Order Moment: Track Duplication and Smearing

Chapter 3

Acknowledgements

I would like to thank my supervisor Prof. Claude Leroy for his guidance, and Dr. Hulya Guler for supervising the factorial moments project. Special thanks to Olivia Scallon for her help on the Medipix project. I would also like to thank the Institute of Particle Physics and the National Science and Engineering Research Council of Canada for funding this research.

Bibliography

[1] C. Albajar et al. Intermittency studies in proton-antiproton collisions at $\sqrt{s} = 630$ GeV. *Nuclear Physics B*, 345:1–21, 1990.

[2] A. Bialas and R. Peschanski. Moments of rapidity distributions as a measure of short-range fluctuations in high-energy collisions. *Nuclear Physics B*, 273:703–718, 1986.

[3] T. H. Burnett et al. Extremely high multiplicities in high-energy nucleus-nucleus collisions. *Phys. Rev. Lett.*, 50:20622065, 1983.

[4] A. Gutierrez. Etude de la réponse du détecteur ATLAS-MPX aux neutrons rapides. Master's thesis, Université de Montréal, Montréal, Canada, 2009.

[5] A. Gutierrez et al. Fast neutron detection efficiency of atlas-mpx detectors for the evaluation of average neutron energy in mixed radiation fields. *Nucl. Instr. and Meth. A*, 2010.

[6] P. Lipa, H. Eggers, F. Botterweck, and M. Charlet. Intermittency, the empty bin effect and uncertainty in factorial moments. *Z. Phys. C - Particles and Fields*, 54:115–125, 1992.

[7] O. Scallon et al. Estimate of the neutron fields in ATLAS based on ATLAS-MPX detectors data. IWORID 2010 Poster Session, 2010.